

Rapid mass growth and enhanced light extinction of atmospheric aerosols during the heating season haze episodes in Beijing revealed by aerosol-chemistry-radiation-boundary layer interaction

Zhuohui Lin¹, Yonghong Wang^{2,3}, Feixue Zheng¹, Ying Zhou¹, Yishuo Guo¹, Zemin Feng¹, Chang Li¹, Yusheng Zhang¹, Simo Hakala², Tommy Chan², Chao Yan², Kaspar R. Daellenbach², Biwu Chu³, Lubna Dada², Juha Kangasluoma^{1,2}, Lei Yao², Xiaolong Fan¹, Wei Du², Jing Cai², Runlong Cai², Tom V. Kokkonen^{2,4}, Putian Zhou², Lili Wang⁵, Tuukka Petäjä^{2,4}, Federico Bianchi^{1,2}, Veli-Matti Kerminen^{2,4}, Yongchun Liu¹, and Markku Kulmala^{1,2,4}

¹Aerosol and Haze Laboratory, Beijing Advanced Innovation Center for Soft Matter Science and Engineering, Beijing University of Chemical Technology, Beijing, China

²Institute for Atmospheric and Earth System Research / Physics, Faculty of Science, University of Helsinki, Finland

³Research Center for Eco-Environmental Sciences, Chinese Academy of Science, Beijing, China

⁴Joint international research Laboratory of Atmospheric and Earth System sciences (JirLATEST), Nanjing University, Nanjing, China

⁵State Key Laboratory of Atmospheric Boundary Layer Physics and Atmospheric Chemistry (LAPC), Institute of Atmospheric Physics, Chinese Academy of Sciences, Beijing 100029, China

Corresponding author: Yonghong Wang

E-mail: yonghongwang@rcees.ac.cn

Revised to: Atmospheric Chemistry and Physics

27 **Abstract**

28

29 Despite the numerous studies investigating haze formation mechanism in China, it is still puzzling
30 that intensive haze episodes could form within hours directly following relatively clean periods. Haze
31 has been suggested to be initiated by the variation of meteorological parameters and then to be
32 substantially enhanced by aerosol-radiation-boundary layer feedback. However, knowledge on the
33 detailed chemical processes and the driving factors for extensive aerosol mass accumulation during
34 the feedback is still scarce. Here, the dependency of the aerosol number size distribution, mass
35 concentration and chemical composition on the daytime mixing layer height (MLH) in urban Beijing
36 is investigated. The size distribution and chemical composition-resolved dry aerosol light extinction
37 is also explored. The results indicate that the aerosol mass concentration and fraction of nitrate
38 increased dramatically when the MLH decreased from high to low conditions, corresponding to
39 relatively clean and polluted conditions, respectively. Particles having their dry diameters in the size
40 of ~400-700 nm, and especially particle-phase ammonium nitrate and liquid water, contributed
41 greatly to visibility degradation during the winter haze periods. The dependency of aerosol
42 composition on the MLH revealed that ammonium nitrate and aerosol water content increased the
43 most during low MLH conditions, which may have further triggered enhanced formation of sulphate
44 and organic aerosol via heterogeneous reactions. As a result, more sulphate, nitrate and water soluble
45 organics were formed, leading to an enhanced water uptake ability and increased light extinction by
46 the aerosols. The results of this study contribute towards a more detailed understanding of the aerosol-
47 chemistry-radiation-boundary layer feedback that is likely to be responsible for explosive aerosol
48 mass growth events in urban Beijing.

49

50

51

52

53

54

55 1. Introduction

56 Despite the recent reduction of air pollutants and their precursors in China between 2013 and 2017,
57 the current emission and air pollution levels are still substantially high (Wang et al., 2020b; Zheng et
58 al., 2018). Such high emissions, combined with specific meteorological conditions, frequently lead
59 to severe haze episodes (An et al., 2019; Wang et al., 2019). Particulate matter, a major air pollutant,
60 has considerable effects on climate, human health and visibility degradation (Che et al., 2007;
61 Lelieveld et al., 2015; Spracklen et al., 2008; Wang et al., 2015).

62
63 During winter haze episodes, a rapid growth of the aerosol mass concentration has commonly been
64 observed, and this phenomenon seems to be directly affected by meteorological factors (Li et al.,
65 2018b; Liu et al., 2018, 2019b; Wang et al., 2018a, 2014a). The meteorological conditions and
66 increased aerosol concentrations are proposed to be interlinked by a feedback loop, called the aerosol-
67 chemistry-boundary layer feedback, in which aerosol particles reduce both solar radiation reaching
68 the surface and turbulent kinetic energy (TKE) of the near-surface air (Ding et al., 2016; Petäjä et al.,
69 2016; Wang et al., 2020d). The reduced TKE owing to aerosol reduce the entrainment of relatively
70 dry air into the mixing layer from above, which makes the air more humid within the mixing layer.
71 The increased relative humidity due to decreased surface temperature enhance the aerosol water
72 uptake ability and promote secondary aerosol formation via aqueous-phase reactions, enhancing light
73 scattering and causing further reduction of solar radiation reaching the surface. All of these factors
74 lead to increased stability of mixing layer height and enhanced air pollution in the mixed layer, which
75 further suppresses the development of boundary layer. As a consequence, concentrations of primary
76 aerosol particles, water vapor and relative humidity increase, creating more favourable conditions for
77 homogeneous and heterogeneous reactions on aerosol surfaces or inside them (Cheng et al., 2016a;
78 Wang et al., 2016; Wu et al., 2018). Such reactions cause rapid formation of secondary aerosol matter
79 and enhanced light extinction during severe winter haze episodes. However, more detailed
80 information on the aerosol and reactive gas chemistry during the aerosol-chemistry-boundary layer
81 feedback and related rapid aerosol mass growth events is still needed (Liu et al., 2019). For instance,
82 it is still unclear which chemical reactions and which compounds in the particulate matter play key

83 roles during such rapid mass growth events.

84

85 The particle number size distribution and chemical composition are considered to be the most
86 important variables influencing the light extinction by aerosol particles. In the atmosphere, the highest
87 contribution to aerosol light extinction comes from organic compounds, nitrate and sulphate in
88 particles with diameters of 100-1000 nm. This is due to the dominant mass fractions of the
89 aforementioned compounds in aerosols that correspond to the peak intensity of solar radiation at
90 wavelengths around 550 nm (Jimenez et al., 2009; Swietlicki et al., 2008). In addition, light scattering
91 which contributes the most to the light extinction by atmospheric aerosols, can be substantially
92 enhanced by the presence of liquid water in the aerosol (Chen et al., 2014; Liu et al., 2019a; Pan et
93 al., 2009; Wang et al., 2020). Hence, quantifying the response of light extinction to different chemical
94 compounds would be helpful in evaluating the feedbacks associated with secondary aerosol
95 production.

96

97 In this study, we focus on the physical and chemical properties of aerosols in Beijing during the winter
98 heating season from October 2018 to February 2019 using state-of-the-art instrumentation. The
99 variation of aerosol chemical composition and the associated light extinction coefficient as a function
100 of the varying mixing layer height are discussed. Our aim is to identify the key chemical components
101 which contribute to the aerosol-chemistry-radiation-boundary layer feedback loop in Beijing.

102

103 **2. Methodology**

104 **2.1. Measurement location and instrumentations**

105 Measurements were conducted between 1 October 2018 and 28 February 2019 at the roof top of the
106 university building at the west campus of Beijing University of Chemical Technology (39.95°N,
107 116.31°E). This station is located about 150 m away from the nearest road (Zizhuyuan road) and 500
108 m away from the West Third Ring Road, and it is surrounded by commercial properties and residential

109 dwellings representative of an urban environment. More details on the location can be found in (Liu
110 et al., 2020; Zhou et al., 2020).

111

112 The meteorological data for this work include basic meteorological variables (relative humidity (RH),
113 temperature, wind speed, wind direction, and visibility) and mixing layer height (MLH) measured
114 using a weather station (Vaisala Inc., Finland) and a Ceilometer CL51 (Vaisala Inc., Finland),
115 respectively. The MLH is defined as the height above the surface, through which relatively vigorous
116 vertical mixing occurs (Holzworth, 1972), and its value is highly related to the vertical temperature
117 structure and, so some extent, to a mechanically-induced turbulence (Baxter, 1991). Here, we
118 followed the method introduced earlier by Münkkel et al. (2007) and Eresmaa et al. (2012) in
119 determining the MLH.

120

121 The number concentration of clusters or small aerosol particles in the size range from 1.3-2.5 nm and
122 the number size distributions of aerosol particles from 6 nm to 840 nm were measured by a Particle
123 Sizer Magnifier (PSM) and a Differential Mobility Particle Sizer (DMPS), respectively (Aalto et al.,
124 2001; Vanhanen et al., 2011). The mass concentration of fine particulate matter (PM_{2.5}) was measured
125 using a Tapered Element Oscillating Microbalance Dichotomous Ambient Particulate Monitor
126 (TEOM 1405-DF, Thermo Fisher Scientific Inc, USA) with a total flow rate of 16.67 L/min (Wang
127 et al., 2014).

128

129 A time-of-flight aerosol chemical speciation monitor (ToF-ACSM, Aerodyne Research Inc.) was used
130 to measure the concentrations of non-refractory (NR) components, including sulfate, nitrate,
131 ammonium, chloride and organics of PM_{2.5} (Fröhlich et al., 2013). A PM_{2.5} cyclone was deployed on
132 the rooftop with a flow rate of 3 L/min. Aerosol was dried though a Nafion dryer (MD-700-24F-3,
133 PERMA PURE) before entering the ToF- ACSM. The inlet flow was set at 1.4 cm³/s. The particle
134 beam passed through the chamber and reached the heated porous tungsten surface (T≈600°C). There,
135 the non-refractory PM_{2.5} constituents were vaporized and then ionized by electrons (E_{kin}=70eV,
136 emitted by a tungsten filament). The ions were measured by a detector and the data was analyzed

137 using Tofware ver. 2.5.13 within IgorPro ver. 6.3.7.2 (WaveMetrics). The relative ionization
138 efficiencies (RIE) for sulfate, nitrate, ammonium, chloride and organics applied were 0.86, 1.05, 4.0,
139 1.5 and 1.4, respectively. Besides RIE correction, the data also did CO₂+/- NO₃ artifact correction
140 (Pieber et al., 2016) and collection efficiency (CE) correction (Middlebrook et al., 2012). Mass
141 concentrations of ammonium nitrate, ammonium sulfate and ammonium chloride were determined
142 according to the method introduced by Gysel et al. (2007). The aerosol liquid water content (AWC)
143 was calculated by the thermodynamic equilibrium model ISORROPIA II using ToF-ACSM data
144 (Fountoukis and Nenes, 2007).

145 Highly-oxygenated organic molecules (HOMs) were measured by a chemical ionization long time-
146 of-flight mass spectrometer equipped with a nitrate chemical ionization source (LToF-CIMS,
147 Aerodyne Research, Inc. USA) (Jokinen et al., 2012) similar to gas-phase sulfuric acid. The ambient
148 air was drawn into the ionization source through a stainless-steel tube with a length of ~1.6 m and a
149 diameter of 3/4 inch at a flowrate of ~ 8 L/min. A 30-40 L/min purified air flow and a 4-8 mL/min
150 ultrahigh purity nitrogen flow containing nitric acid were mixed together as the sheath flow, which is
151 guided through a PhotoIonizer (Model L9491, Hamamatsu, Japan) to produce nitrate reagent ions.
152 This sheath flow is then introduced into a co-axial laminar flow reactor concentric to the sample flow.
153 Nitrate ions are pushed to the sample flow layer by an electric field and subsequently charge analytical
154 molecules. Organic carbon (OC) and element carbon (EC) concentrations were measured semi-
155 continuously with a 1-hour time resolution using an OC/EC Analyzer (Model-4, Sunset Lab. Inc.).
156 The ammonia is measured by Trace Ammonia analyzer (Los Gatos Research, Inc.) at atmospheric
157 ambient levels with high precision (0.2 ppb in 1s) and ultra-fast response (5 Hz).

158

159 The air mass history was studied by calculating particle retroplumes using a Lagrangian particle
160 dispersion model FLEXPART (FLEXible PARTicle dispersion model) ver. 9.02 (Stohl et al., 2005).
161 The ECMWF (European Centre for Medium-Range Weather Forecast) operational forecast (with 0.15°
162 horizontal and 1 h temporal resolution) was used as the meteorological input into the model. During
163 the measurement period, a new release of 50 000 test particles, distributed evenly between 0 and 100
164 m above the measurement site, occurred every 1 hour. The released particles were traced backwards

165 in time for 72 h, unless they exceeded the model boundary (20–60°N, 95–135°E).

166

167 2.2. Aerosol light extinction calculation

168 The aerosol light extinction coefficient was calculated with the Mie-Model, which uses particle
169 number size distribution, mass concentrations of different aerosol compounds and their refractive
170 index as inputs (Seinfeld and Pandis, 2006). We introduced a series of assumptions into the Mie-
171 Model, including 1) “internal mixture” which considers each chemical component in a particle as
172 homogeneously mixed with each other; 2) all particles are spherical; and 3) particles of different sizes
173 have the same chemical composition.

174

175 The practical method introduced under those assumptions in previous studies were found to be
176 capable of estimating a variation trend of optical property of PM_{0.5–20} with a relatively good accuracy
177 (Lin et al., 2013).

178

179 Table 1. Summary of the parameters for calculating the average optical refractive index.

180

Species	$\rho_i (\text{g cm}^{-3})$	n_i	k_i
(NH ₄) ₂ SO ₄	1.760	1.530	0.000
NH ₄ NO ₃	1.725	1.554	0.000
NH ₄ Cl	1.527	1.639	0.000
Organics	1.400	1.550	0.001
EC	1.500	1.800	0.540

181

182 The average optical refractive index (AORI) of an internally-mixed particle can be calculated from
183 the optical refractive indices (ORI) of each chemical component by following a mixing rule of
184 volume-averaged chemical components as $\text{AORI} = n_{\text{eff}} + k_{\text{eff}} \times i$, where the real part (n_{eff}) and
185 imaginary part (k_{eff}) are given by:

$$n_{eff} = \left(\sum_i n_i \cdot m_i / \rho_i \right) / \left(\sum_i m_i / \rho_i \right) \quad (1)$$

$$k_{eff} = \left(\sum_i k_i \cdot m_i / \rho_i \right) / \left(\sum_i m_i / \rho_i \right) \quad (2)$$

Here m_i and ρ_i are the mass concentration and density of the component i in particles, respectively, and n_i and k_i are the real and imaginary parts of ORI of this component, respectively. The parameters for calculating the AORI are summarised in Table 1. The values of n_i and k_i in Table 1 are referenced to the light wavelength of 550 nm.

$Q_{sp,j}$ represents light scattering efficiency of a single particle with diameter D_j , while $Q_{ep,j}$ represents light absorption efficiency. Theoretically, $Q_{sp,j}$ and $Q_{ep,j}$ are both the function of D_j and the $AORI_j$ (the AORI of the particle with diameter D_j) at a given light wavelength λ , for which the complicated calculations were referenced to a previous publication (Lin et al., 2013). Regarding the limitations of measurement techniques, the $AORI_j$ was assumed to be equal to the $AORI_{PM2.5}$, which was determined based on chemical composition of $PM_{2.5}$. It is possible to derive expressions for the cross sections of a spherical particle exactly. The formulas for $Q_{sp,j}$ and $Q_{ep,j}$ are:

$$Q_{sp,j}(D_j, \lambda, AORI_j) = \frac{2}{\alpha^2} \sum_{k=1}^{\infty} (2k+1) \cdot [|a_k|^2 + |b_k|^2] \quad (3)$$

$$Q_{ep,j}(D_j, \lambda, AORI_j) = \frac{2}{\alpha^2} \sum_{k=1}^{\infty} (2k+1) \cdot Re[a_k + b_k] \quad (4)$$

where

$$a_k = \frac{\alpha \psi'_k(y) \psi_k(\alpha) - y \psi'_k(\alpha) \psi_k(y)}{\alpha \psi'_k(y) \xi_k(\alpha) - y \xi'_k(\alpha) \psi_k(y)}$$

$$b_k = \frac{y \psi'_k(y) \psi_k(\alpha) - \alpha \psi'_k(\alpha) \psi_k(y)}{y \psi'_k(y) \xi_k(\alpha) - \alpha \xi'_k(\alpha) \psi_k(y)}$$

206 with $y = \alpha m$.

207

$$208 \quad m = n_{eff} + i \cdot k_{eff}$$

209

$$210 \quad \alpha = \frac{\pi D_j}{\lambda}$$

211

212 with $\lambda = 550$ nm.

213

214 where complex number m stands for $AORI_j$, while α is the size of the particle, usually expressed as
215 a dimensionless size parameter. The functions $\psi_k(z)$ and $\xi_k(z)$ are the Riccati–Bessel functions:

$$\psi_k(z) = \left(\frac{\pi z}{2}\right)^{1/2} J_{k+1/2}(z) \quad (5)$$

$$\xi_k(z) = \left(\frac{\pi z}{2}\right)^{1/2} [J_{k+1/2}(z) + i(-1)^k J_{-k-1/2}(z)] \quad (6)$$

216

217 where $J_{k+1/2}$ and $J_{-k-1/2}$ are the Bessel functions of the first kind and their footnotes indicate the
218 order of Bessel functions. The Mie theory can serve as the basis of a computational procedure to
219 calculate the scattering and absorption of light by any sphere as a function of wavelength.

220

221 According to the Mie-Model, b_{sp} (light scattering coefficient) and b_{ep} (light extinction coefficient)
222 can be quantified with Eqs. (5) and (6), respectively. b_{ap} (light absorption coefficient) is the
223 difference between b_{ep} and b_{sp} , which equals zero, when k_i equals zero or very small. Optical
224 properties including b_{ep} , b_{sp} and b_{ap} to be discussed later are all referenced to light wavelength of
225 550 nm.

$$b_{sp} = \sum_j b_{sp,j} = \sum_j \frac{\pi D_j^2}{4} \cdot Q_{sp,j}(D_j, \lambda, AORI_j) \cdot N_j \quad (7)$$

$$b_{ep} = \sum_j b_{ep,j} = \sum_j \frac{\pi D_j^2}{4} \cdot Q_{ep,j}(D_j, \lambda, AORI_j) \cdot N_j \quad (8)$$

226

227

228 In Eqs. (7) and (8), D_j stands for the median Stokes diameter in the j -th particle size range and N_j is
229 the number concentration of particles with diameter, D_j .

230

231 3. Results and discussion

232 3.1. Typical case of rapid aerosol mass growth episodes affected by aerosol-chemistry- 233 boundary layer interactions

234 An example of rapid aerosol mass growth in urban wintertime Beijing is illustrated in Figure 1, where
235 the haze accumulation was associated with a rapid $PM_{2.5}$ mass concentration increase from $8.5 \mu g/m^3$
236 to more than $100 \mu g/m^3$ in less than 7 hours. A haze episode started on afternoon 20 February 2019
237 under stagnant meteorological conditions with low wind speeds and elevated ambient relative
238 humidity (Figure S1). The polluted periods during this case occurred under southerly wind transport
239 conditions, whereas clean air masses originated from the north-westerly regions (as shown in Figure
240 S2, S3). These are typical features for a haze evolution process in Beijing (Wang et al., 2020b). During
241 the haze periods marked by the shaded areas in Figure 1, an obvious increase of chemical mass
242 concentration was observed by the ToF-ACSM, characterised by high concentrations of secondary
243 aerosol components (nitrate, organics and sulphate) and typically a shallow boundary layer. The mass
244 concentrations of organics, sulphate and nitrate increased dramatically with a decreasing MLH,
245 accounting for 88.5% of NR- $PM_{2.5}$ (non-refractory $PM_{2.5}$) during the rapid aerosol mass growth
246 period. The aerosol mass growth was the fastest for nitrate. The mass concentrations of organic and
247 elemental carbon followed that of NR- $PM_{2.5}$.

248

249 The MLH reached its maximum at around 14:00 in the afternoon of 20 February, after which the
250 development of the mixing layer was suppressed and MLH decreased with the arrival of pollution
251 (Figure 1a). Previous studies have shown that the aerosol-radiation-boundary layer feedback
252 contributes to a rapid enhancement of air pollution (Petäjä et al., 2016; Wang et al., 2020d). High

concentrations of aerosol particles obscure downward radiation, as a result of which the surface temperature and sensitive heat flux decrease and the development of mixing layer height is suppressed. Recent studies have gradually realized that the facilitation of various chemical processes play a non-negligible role in the aerosol-radiation-boundary layer feedback (Liu.Q et al., 2018; Liu. Z et al.,2019). Therefore, it is important to identify and quantify the role of different specific chemical species and particle size ranges in reducing atmospheric radiation and extinction.

Figure 2 shows the contributions of size and chemical composition-resolved dry aerosol to light extinction during the investigated period. As the pollution intensified and MLH decreased (Fig 1c), the light extinction of atmospheric aerosols increased significantly. Assuming that particles of different sizes have the same chemical composition as PM_{2.5} (organics, NH₄NO₃, EC, (NH₄)₂SO₄, NH₄Cl), the light extinction of particles in the size range of 300-700 nm increased significantly from the relative clean period to the polluted period (namely from 12:00 to 16:00). During relatively clean conditions, the contributions of organics, NH₄NO₃, EC, (NH₄)₂SO₄ and NH₄Cl to the total aerosol light extinction were 42%, 23%, 18%, 11% and 7%, respectively. The contribution of NH₄NO₃ to aerosol light extinction reached 40% during the heavily polluted period. Based on the observation it is likely that the increased light extinction by aerosols reduced solar radiation reaching the surface, so that the development of the boundary layer was suppressed.

3.2. Connection between the aerosol chemical composition, light extinction, size distribution and MLH during the heating season

To better characterize the effect of the chemical composition of dry aerosols and the PNSD (particle number size distribution) light extinction under different MLH conditions, the daytime (8:00 – 16:00 LT) measurement data from October 2018 to February 2019 were selected for further analysis. As shown by Figure 3 and consistent with other observations in Beijing (Tang et al., 2016; Wang et al., 2020c), there was a general tendency for the PM_{2.5} mass concentration to increase with a decreasing

280 MLH. Organic compounds and nitrate were the most abundant fractions of the daytime aerosol mass
281 composition, contributing together approximately 70% to total NR-PM_{2.5} mass concentration. With a
282 decreasing MLH, the fraction of nitrate mass in NR-PM_{2.5} slightly increased while that of organics
283 decreased. This feature makes the aerosol more hygroscopic under low MLH conditions typical for
284 heavily polluted periods. The increased nitrate fraction in the aerosol could also enhance the
285 formation of other secondary aerosol components (Xue et al., 2019). Note that some fraction of
286 aerosol nitrate could consist of organic nitrate originating from reaction of peroxy radical with nitric
287 oxide; however, it is difficult to distinguish organic nitrate from inorganic nitrate at the moment due
288 to instrumental limitations (Fröhlich et al., 2013).

289

290 Figure 4 depicts the calculated daytime light extinction of the dry aerosol as a function of the MLH,
291 separated by different size ranges and chemical components. We may see that in general, particles
292 with dry diameters in the range of 300-700 nm explains more than 80% of the total aerosol light
293 extinction (Figure 4b). Similar to their share in NR-PM_{2.5}, the fraction of light extinction by
294 ammonium nitrate increased and that of organics decreased during the lowest MLH conditions
295 corresponding to the heavy pollution periods (Figure 4d). There are also apparent differences in the
296 relative contribution of different particle size ranges to light extinction in different MLH conditions:
297 with a decreasing MLH, the contribution of particles with dry dimeters larger than about 400-500 nm
298 clearly increased while that of sub-300 nm particles notably decreased. This indicates that the
299 enhanced light extinction by the dry aerosol at low MLH conditions was not only due the more
300 abundant aerosol mass concentration, but also due to the growth of individual particles to optically
301 more active sizes.

302

303 At relative humidity larger than about 70%, aerosol liquid water gives a significant contribution to
304 the aerosol mass concentration and often a dominant contribution to the aerosol light extinction (Titos
305 et al., 2016). This has important implications for the aerosol-chemistry-radiation-boundary layer
306 feedback, when considering our findings listed above and further noting that heavy pollution periods
307 are often accompanied by high values of RH in Beijing (Zhong et al., 2018). First, compared to clean

308 or moderately-polluted conditions, the enhancement in the aerosol light extinction under polluted is
309 probably much larger than that illustrated in Figure 4. Second, the high aerosol water content under
310 polluted conditions promotes many kinds of chemical reactions taking place on the surface or inside
311 aerosol particles.

312

313 **3.3. Aerosol-chemistry-radiation-boundary layer interaction**

314

315 In order to further investigate the interaction between MLH and chemical compounds (either observed
316 or calculated), we divided the observed PM_{2.5} concentrations into highly polluted and less polluted
317 conditions using a threshold value of 75 µg /m³ for PM_{2.5}. The organics, nitrate, ammonium, sulfate,
318 chloride, HOM, aerosol water content (AWC) and PM_{2.5} as a function of the mixing layer height
319 during both highly polluted and less polluted conditions are shown in Figure 5. The fitted relationships
320 connecting the concentrations of different chemical compounds to the reduction of MLH under highly
321 and less polluted conditions allowed us to estimate the net mass concentration increase of each
322 compound due to secondary formation and aerosol-chemical-boundary layer feedback under highly
323 polluted conditions (shaded areas in Figure 5). It is worth noting that AWC, nitrate and sulfate
324 increased the most as the MLH decreased, as represented by the large shaded areas in Figs. 5 (h), (b)
325 and (c). The day-time nitrate in aerosol is formed predominately via the reaction of nitric acid and
326 ammonium, while nitric acid is produced from gas phase reaction of nitrogen dioxide and hydroxy
327 radical (Seinfeld and Pandis, 2006). High concentrations of daytime nitrate aerosols indicate efficient
328 production of gas phase nitric acid, its partitioning into liquid aerosol and its fast neutralization by
329 abundant ammonia (Li et al., 2018a; Pan et al., 2016; Wang et al., 2020). A recent study shows that
330 condensation of nitric acid and ammonia could promote fast growth of newly formed particle in urban
331 environment condition (Wang et al., 2020d). Another possibility is that ammonium nitrate is formed
332 rapidly on particle surfaces due to the hydrolysis of dinitrogen pentoxide (N₂O₅) during daytime, as
333 the AWC increased significantly (Wang et al., 2014; Wang et al., 2020). However, a quantitative
334 distinction between the two formation pathways for nitrate formation is not possible in this study. The

dramatic increase of nitrate aerosol could also promote the formation of sulfate by heterogeneous reactions (Cheng et al., 2016b; Wang et al., 2016). The concentration of HOMs showed a slight increase as the MLH decreased, which suggests that also the formation of HOMs is enhanced with an increased level of air pollution. This phenomenon should be further investigated as HOMs can substantially contribute to the secondary organic aerosol formation.

Figure 6 displays the dry aerosol light extinction by different chemical compounds in the same way as Fig. 5 did for aerosol mass concentrations. The aerosol light extinction is directly related to the reduction of solar radiation reaching the surface, assuming that aerosol chemical components are vertically nearly homogeneously distributed. The light extinction from ammonium nitrate, ammonium sulfate and organics showed significantly increased contributions under highly polluted conditions (low MLH) as compared with less polluted conditions. To the contrary, no such enhancement was observed for ammonium chloride or element carbon (Figs. 6 (d) and (e)). In case of EC this is an expected result, as it originates solely from primary sources. The formation of particle phase chloride have secondary sources from chlorine atom-initiated oxidation of volatile organic compounds, so that the resulting oxidation products could contribute to the observed chloride (Wang and Ruiz, 2017; Wang et al., 2019a).

To better illustrate the combined effects of secondary aerosol formation and associated feedback on the daytime mass concentrations and light extinction due to different chemical components, we scaled these quantities by either the total $PM_{2.5}$ mass concentration or EC concentration and plotted them as a function of MLH (Fig. 7). The latter scaling minimizes the boundary layer accumulation effect on our analysis, as EC originates from primary emission sources (Cao et al., 2006). As shown in Fig. 7a, organics with their mass fraction of 61% were the most abundant component in $PM_{2.5}$ under high MLH conditions, followed by nitrate and ammonium with their mass fractions of 22% and 13%, respectively. The aerosol was estimated to be rather dry under high MLH conditions ($AWC/PM_{2.5} = 0.03$). However, with the decreasing MLH, the fraction of nitrate and the AWC to $PM_{2.5}$ ratio increased up to 45% and 0.2, respectively. This clearly indicates rapid nitrate formation and dramatic increase

363 of the aerosol water uptake from less polluted conditions to intensive haze pollution. Compared with
364 EC (Fig.7c), the concentrations of organic compounds, nitrate, sulfate and ammonium increased by
365 factors of 1.5, 6.3, 4.8 and 4.9 respectively, from the highest to the lowest MLH conditions. Thus,
366 although organics remained as the second most abundant aerosol component after nitrate under haze
367 conditions, secondary formation and associated feedback from less to highly polluted conditions were
368 clearly stronger for both sulfate and ammonium. Efficient sulfate production associated with haze
369 formation has been reported in several studies conducted in China (Cheng et al., 2016; Xie et al.,
370 2015; Xue et al., 2016). Ammonium production during haze formation is tied with neutralization of
371 acidic aerosol by ammonia, which was apparently present abundantly in the gas phase. Compared
372 with the EC concentration, light extinction by (NH_4NO_3) increased the most from the highest MLH
373 conditions ($248 \text{ M m}^{-1}/\mu\text{g m}^{-3}$) to the lowest MLH conditions ($1150 \text{ M m}^{-1}/\mu\text{g m}^{-3}$) as shown by Figure
374 7b. Overall, the rapid growth of nitrate aerosol mass, together with abundant concentration of organic
375 aerosol, were the main cause of the light extinction for dry aerosol under haze formation.

376

377 The mechanism governing the aerosol-chemistry-radiation-boundary layer feedback for the rapid
378 growth of atmospheric aerosol is illustrated in Fig. 8. As a result of reduction in solar radiation and
379 atmospheric heating, a variety of chemical reactions in the gas phase and on particle surfaces or inside
380 them are enhanced with an increased relative humidity and AWC. Such conditions are unfavorable
381 for the dispersion of pollutants, which further enhances atmospheric stability. The formation of
382 hydrophilic compounds, e.g., nitrate, sulfate and oxygenated organic compounds, result in enhanced
383 water uptake by aerosol particles, which will essentially increase heterogeneous reactions associated
384 with these particles. As a result, the aerosol mass and size increase, light extinction is enhanced, and
385 the development of the mixing layer is depressed. At the same time, aerosol precursors concentrated
386 within a shallower mixing layer lead to enhanced production rate of aerosol components in both gas
387 and aerosol phases, especially nitrate but also other secondary aerosol. The increased concentrations
388 of aerosol will further enhance this positive loop.

389

390 4. Conclusions

391

392 We investigated the synergetic variations of aerosol chemical composition and mixing layer height
393 during the daytime in urban Beijing. Significant dependency of the sharp increase of ammonium
394 nitrate and aerosol water content with the occurrence of the explosive aerosol mass growth events
395 were observed. We showed that these two components drove a positive aerosol-chemistry-radiation-
396 boundary layer feedback loop, which played an important role in the explosive aerosol mass growth
397 events. A plausible explanation is that the increased aerosol water content at low mixing layer heights
398 provides favorable conditions for heterogeneous reactions for nitrate and sulfate production and
399 neutralization by ammonia. The significant formation of secondary aerosol increases the
400 concentration of aerosol particles in the diameter range 300-700 nm, which effectively reduces the
401 solar radiation reaching the surface and further enhances the aerosol-chemistry-radiation-boundary
402 layer feedback loop. Our analysis connects the aerosol light extinction to a reduction in the mixing
403 layer height, which suppresses the volume into which air pollutants are emitted and leads to an
404 explosive aerosol mass growth. Our results indicate that reduction of ammonium and nitrate
405 concentration in aerosol could weaken the aerosol-radiation-chemistry-boundary layer feedback loop,
406 which could thereby reduce heavy haze episodes in Beijing.

407 5. Acknowledgements

408 This work was supported by the funding from Beijing University of Chemical Technology. The
409 European Research Council via advanced grant ATM-GTP (project no. 742206) and Academy of
410 Finland via Academy professor project of M. K.

411 6. Competing financial interests

412 The authors declare no competing financial interests.

7. Author contributions

413 YW and MK initiated the study. ZL, YW, FZ, YZ, YG, ZF, CL, YZ, TC, CY, KD, BC, JK, LY, XF,
414 WD, JC and YL conducted the longtime measurements. ZL, YW, LD, RC, SH, PZ, LW, VK, YL and
415 MK interpreted the data. ZL, YW and VK wrote the manuscript.

416

417

418

419

- Aalto, P., Hämeri, K., Becker, E. D. O., Weber, R., Salm, J., Mäkelä, J. M., Hoell, C., O'Dowd, C. D., Karlsson, H., Hansson, H., Väkevä, M., Koponen, I. K., Buzorius, G. and Kulmala, M.: Physical characterization of aerosol particles during nucleation events, *Tellus, Series B: Chemical and Physical Meteorology*, 53(4), 344–358, doi:10.3402/tellusb.v53i4.17127, 2001.
- An, Z., Huang, R.-J., Zhang, R., Tie, X., Li, G., Cao, J., Zhou, W., Shi, Z., Han, Y., Gu, Z. and Ji, Y.: Severe haze in northern China: A synergy of anthropogenic emissions and atmospheric processes, *Proceedings of the National Academy of Sciences*, 116(18), 8657 LP – 8666, doi:10.1073/pnas.1900125116, 2019.
- Baxter, R.: Determination of mixing heights from data collected during the 1985 SCCCAMP field program, *Journal of Applied Meteorology*, 30(5), 598–606, doi:10.1175/1520-0450(1991)030<0598:DOMHFD>2.0.CO;2, 1991.
- Cao, G., Zhang, X. and Zheng, F.: Inventory of black carbon and organic carbon emissions from China, *Atmospheric Environment*, 40(34), 6516–6527, doi:10.1016/j.atmosenv.2006.05.070, 2006.
- Che, H., Zhang, X., Li, Y., Zhou, Z. and Qu, J. J.: Horizontal visibility trends in China 1981-2005, *Geophysical Research Letters*, 34(24), doi:10.1029/2007GL031450, 2007.
- Chen, J., Zhao, C. S., Ma, N. and Yan, P.: Aerosol hygroscopicity parameter derived from the light scattering enhancement factor measurements in the North China Plain, *Atmos. Chem. Phys*, 14, 8105–8118, doi:10.5194/acp-14-8105-2014, 2014.
- Cheng, Y., Zheng, G., Wei, C., Mu, Q., Zheng, B., Wang, Z., Gao, M., Zhang, Q., He, K., Carmichael, G., Pöschl, U. and Su, H.: Reactive nitrogen chemistry in aerosol water as a source of sulfate during haze events in China, *Science Advances*, 2(12), e1601530–e1601530, doi:10.1126/sciadv.1601530, 2016b.
- Ding, A. J., Huang, X., Nie, W., Sun, J. N., Kerminen, V. M., Petäjä, T., Su, H., Cheng, Y. F., Yang, X. Q., Wang, M. H., Chi, X. G., Wang, J. P., Virkkula, A., Guo, W. D., Yuan, J., Wang, S. Y., Zhang, R. J., Wu, Y. F., Song, Y., Zhu, T., Zilitinkevich, S., Kulmala, M. and Fu, C. B.: Enhanced haze pollution by black carbon in megacities in China, *Geophysical Research Letters*, 43(6), 2873–2879, doi:10.1002/2016GL067745, 2016.

Eresmaa, N., Härkönen, J., Joffre, S. M., Schultz, D. M., Karppinen, A. and Kukkonen, J.: A Three-Step Method for Estimating the Mixing Height Using Ceilometer Data from the Helsinki Testbed, *Journal of Applied Meteorology and Climatology*, 51(12), 2172–2187, doi:10.1175/JAMC-D-12-058.1, 2012.

Fountoukis, C. and Nenes, A.: ISORROPIA II: a computationally efficient thermodynamic equilibrium model for

K^+ – Ca^{2+} – Mg^{2+} – NH_4^+ – Na^+ – SO_4^{2-} – NO_3 , *Atmospheric Chemistry and Physics*, 7(17), 4639–4659, doi:10.5194/acp-7-4639-2007, 2007.

Fröhlich, R., Cubison, M. J., Slowik, J. G., Bukowiecki, N., Prévôt, A. S. H., Baltensperger, U., Schneider, J., Kimmel, J. R., Gonin, M., Rohner, U., Worsnop, D. R. and Jayne, J. T.: The ToF-ACSM: A portable aerosol chemical speciation monitor with TOFMS detection, *Atmospheric Measurement Techniques*, 6(11), 3225–3241, doi:10.5194/amt-6-3225-2013, 2013.

Gysel, M., Crosier, J., Topping, D. O., Whitehead, J. D., Bower, K. N., Cubison, M. J., Williams, P. I., Flynn, M. J., McFiggans, G. B. and Coe, H.: Closure study between chemical composition and hygroscopic growth of aerosol particles during TORCH2, *Atmospheric Chemistry and Physics*, 7(24), 6131–6144, doi:10.5194/acp-7-6131-2007, 2007.

Holzworth, G. C.: Mixing heights, wind speeds, and potential for urban air pollution throughout the contiguous united states, , 118, 1972.

Jimenez, J. L., Canagaratna, M. R., Donahue, N. M., Prevot, A. S. H., Zhang, Q., Kroll, J. H., DeCarlo, P. F., Allan, J. D., Coe, H., Ng, N. L., Aiken, A. C., Docherty, K. S., Ulbrich, I. M., Grieshop, A. P., Robinson, A. L., Duplissy, J., Smith, J. D., Wilson, K. R., Lanz, V. A., Hueglin, C., Sun, Y. L., Tian, J., Laaksonen, A., Raatikainen, T., Rautiainen, J., Vaattovaara, P., Ehn, M., Kulmala, M., Tomlinson, J. M., Collins, D. R., Cubison, M. J., Dunlea, E. J., Huffman, J. A., Onasch, T. B., Alfarra, M. R., Williams, P. I., Bower, K., Kondo, Y., Schneider, J., Drewnick, F., Borrmann, S., Weimer, S., Demerjian, K., Salcedo, D., Cottrell, L., Griffin, R., Takami, A., Miyoshi, T., Hatakeyama, S., Shimojo, A., Sun, J. Y., Zhang, Y. M., Dzepina, K., Kimmel, J. R., Sueper, D., Jayne, J. T., Herndon, S. C., Trimborn, A. M., Williams, L. R., Wood, E. C., Middlebrook, A. M., Kolb, C. E., Baltensperger, U. and Worsnop, D. R.: Evolution of organic

aerosols in the atmosphere, *Science*, 326(5959), 1525–1529, doi:10.1126/science.1180353, 2009.

Jokinen, T., Sipilä, M., Junninen, H., Ehn, M., Lönn, G., Hakala, J., Petäjä, T., Mauldin, R. L., Kulmala, M. and Worsnop, D. R.: Atmospheric sulphuric acid and neutral cluster measurements using CI-API-TOF, *Atmospheric Chemistry and Physics*, 12(9), 4117–4125, doi:10.5194/acp-12-4117-2012, 2012.

Lelieveld, J., Evans, J. S., Fnais, M., Giannadaki, D. and Pozzer, A.: The contribution of outdoor air pollution sources to premature mortality on a global scale, *Nature*, 525(7569), 367–371, doi:10.1038/nature15371, 2015.

Li, H., Zhang, Q., Zheng, B., Chen, C., Wu, N., Guo, H., Zhang, Y., Zheng, Y., Li, X. and He, K.: Nitrate-driven urban haze pollution during summertime over the North China Plain, *Atmospheric Chemistry and Physics*, 18(8), 5293–5306, doi:10.5194/acp-18-5293-2018, 2018a.

Li, J., Sun, J., Zhou, M., Cheng, Z., Li, Q., Cao, X. and Zhang, J.: Observational analyses of dramatic developments of a severe air pollution event in the Beijing area, *Atmospheric Chemistry and Physics*, 18(6), 3919–3935, doi:10.5194/acp-18-3919-2018, 2018b.

Lin, Z. J., Tao, J., Chai, F. H., Fan, S. J., Yue, J. H., Zhu, L. H., Ho, K. F. and Zhang, R. J.: Impact of relative humidity and particles number size distribution on aerosol light extinction in the urban area of Guangzhou, *Atmospheric Chemistry and Physics*, 13(3), 1115–1128, doi:10.5194/acp-13-1115-2013, 2013.

Liu, G., Xin, J., Wang, X., Si, R., Ma, Y., Wen, T., Zhao, L., Zhao, D., Wang, Y. and Gao, W.: Impact of the coal banning zone on visibility in the Beijing-Tianjin-Hebei region, *Science of the Total Environment*, 692, 402–410, doi:10.1016/j.scitotenv.2019.07.006, 2019a.

Liu, Q., Jia, X., Quan, J., Li, J., Li, X., Wu, Y., Chen, D., Wang, Z. and Liu, Y.: New positive feedback mechanism between boundary layer meteorology and secondary aerosol formation during severe haze events, *Scientific Reports*, 8(1), doi:10.1038/s41598-018-24366-3, 2018.

Liu, Y., Zhang, Y., Lian, C., Yan, C. and Feng, Z.: The promotion effect of nitrous acid on aerosol formation in wintertime Beijing : possible contribution of traffic-related emission, *Atmos. Chem. Phys. Discuss.*, 2020(February), 1–43, doi:10.5194/acp-2020-150, 2020.

Liu, Z., Hu, B., Ji, D., Cheng, M., Gao, W., Shi, S., Xie, Y., Yang, S., Gao, M., Fu, H., Chen, J. and

- Wang, Y.: Characteristics of fine particle explosive growth events in Beijing, China: Seasonal variation, chemical evolution pattern and formation mechanism, *Science of the Total Environment*, 687, 1073–1086, doi:10.1016/j.scitotenv.2019.06.068, 2019b.
- Münkel, C., Eresmaa, N., Räsänen, J. and Karppinen, A.: Retrieval of mixing height and dust concentration with lidar ceilometer, *Boundary-Layer Meteorology*, 124(1), 117–128, doi:10.1007/s10546-006-9103-3, 2007.
- Pan, X. L., Yan, P., Tang, J., Ma, J. Z., Wang, Z. F., Gbaguidi, A. and Sun, Y. L.: Observational study of influence of aerosol hygroscopic growth on scattering coefficient over rural area near Beijing mega-city, *Atmospheric Chemistry and Physics*, 9(19), 7519–7530, doi:10.5194/acp-9-7519-2009, 2009.
- Pan, Y., Tian, S., Liu, D., Fang, Y., Zhu, X., Zhang, Q., Zheng, B., Michalski, G. and Wang, Y.: Fossil Fuel Combustion-Related Emissions Dominate Atmospheric Ammonia Sources during Severe Haze Episodes: Evidence from ^{15}N -Stable Isotope in Size-Resolved Aerosol Ammonium, *Environmental Science and Technology*, 50(15), 8049–8056, doi:10.1021/acs.est.6b00634, 2016.
- Petäjä, T., Järvi, L., Kerminen, V. M., Ding, A. J., Sun, J. N., Nie, W., Kujansuu, J., Virkkula, A., Yang, X., Fu, C. B., Zilitinkevich, S. and Kulmala, M.: Enhanced air pollution via aerosol-boundary layer feedback in China, *Scientific Reports*, 6, doi:10.1038/srep18998, 2016.
- Pieber, S. M., El Haddad, I., Slowik, J. G., Canagaratna, M. R., Jayne, J. T., Platt, S. M., Bozzetti, C., Daellenbach, K. R., Fröhlich, R., Vlachou, A., Klein, F., Dommen, J., Miljevic, B., Jiménez, J. L., Worsnop, D. R., Baltensperger, U. and Prévôt, A. S. H.: Inorganic Salt Interference on CO_2^+ in Aerodyne AMS and ACSM Organic Aerosol Composition Studies, *Environmental Science and Technology*, 50(19), 10494–10503, doi:10.1021/acs.est.6b01035, 2016.
- Spracklen, D. V., Carslaw, K. S., Kulmala, M., Kerminen, V. M., Sihto, S. L., Riipinen, I., Merikanto, J., Mann, G. W., Chipperfield, M. P., Wiedensohler, A., Birmili, W. and Lihavainen, H.: Contribution of particle formation to global cloud condensation nuclei concentrations, *Geophysical Research Letters*, 35(6), doi:10.1029/2007GL033038, 2008.
- Stohl, A., Forster, C., Frank, A., Seibert, P. and Wotawa, G.: Technical note: The Lagrangian particle dispersion model FLEXPART version 6.2, *Atmospheric Chemistry and Physics*, 5(9),

2461–2474, doi:10.5194/acp-5-2461-2005, 2005.

Swietlicki, E., Hansson, H.-C., Hämeri, K., Svenningsson, B., Massling, A., Mcfiggans, G., McMurry, P. H., Petäjä, T., Tunved, P., Gysel, M., Topping, D., Weingartner, E., Baltensperger, U., Rissler, J., Wiedensohler, A. and Kulmala, M.: Hygroscopic properties of submicrometer atmospheric aerosol particles measured with H-TDMA instruments in various environments—a review, *Tellus B: Chemical and Physical Meteorology*, 60(3), 432–469, doi:10.1111/j.1600-0889.2008.00350.x, 2008.

Tang, G., Zhang, J., Zhu, X., Song, T., Munkel, C., Hu, B., Schäfer, K., Liu, Z., Zhang, J., Wang, L., Xin, J., Suppan, P. and Wang, Y.: Mixing layer height and its implications for air pollution over Beijing, China, *Atmos. Chem. Phys*, 16, 2459–2475, doi:10.5194/acp-16-2459-2016, 2016.

Titos, G., Cazorla, A., Zieger, P., Andrews, E., Lyamani, H., Granados-Muñoz, M. J., Olmo, F. J. and Alados-Arboledas, L.: Effect of hygroscopic growth on the aerosol light-scattering coefficient: A review of measurements, techniques and error sources, *Atmospheric Environment*, 141, 494–507, doi:10.1016/j.atmosenv.2016.07.021, 2016.

Vanhanen, J., Mikkilä, J., Lehtipalo, K., Sipilä, M., Manninen, H. E., Siivola, E., Petäjä, T. and Kulmala, M.: Particle size magnifier for nano-CN detection, *Aerosol Science and Technology*, 45(4), 533–542, doi:10.1080/02786826.2010.547889, 2011.

Wang, G., Zhang, R., Gomez, M. E., Yang, L., Zamora, M. L., Hu, M., Lin, Y., Peng, J., Guo, S., Meng, J., Li, J., Cheng, C., Hu, T., Ren, Y., Wang, Y., Gao, J., Cao, J., An, Z., Zhou, W., Li, G., Wang, J., Tian, P., Marrero-Ortiz, W., Secrest, J., Du, Z., Zheng, J., Shang, D., Zeng, L., Shao, M., Wang, W., Huang, Y., Wang, Y., Zhu, Y., Li, Y., Hu, J., Pan, B., Cai, L., Cheng, Y., Ji, Y., Zhang, F., Rosenfeld, D., Liss, P. S., Duce, R. A., Kolb, C. E. and Molina, M. J.: Persistent sulfate formation from London Fog to Chinese haze, *Proceedings of the National Academy of Sciences of the United States of America*, 113(48), 13630–13635, doi:10.1073/pnas.1616540113, 2016.

Wang, H., Peng, Y., Zhang, X., Liu, H., Zhang, M., Che, H. and Cheng, Y.: Contributions to the explosive growth of PM_{2.5} mass due to aerosol – radiation feedback and decrease in turbulent diffusion during a red alert heavy haze in Beijing – Tianjin – Hebei, China, , 17717–17733, 2018a.

Wang, J., Wang, S., Jiang, J., Ding, A., Zheng, M., Zhao, B., Wong, D. C., Zhou, W., Zheng, G.,

Wang, L., Pleim, J. E. and Hao, J.: Impact of aerosol-meteorology interactions on fine particle pollution during China's severe haze episode in January 2013, *Environmental Research Letters*, 9(9), doi:10.1088/1748-9326/9/9/094002, 2014a.

Wang, M., Kong, W., Marten, R., He, X.-C., Chen, D., Pfeifer, J., Heitto, A., Kontkanen, J., Dada, L., Kürten, A., Yli-Juuti, T., Manninen, H. E., Amanatidis, S., Amorim, A., Baalbaki, R., Baccarini, A., Bell, D. M., Bertozzi, B., Bräkling, S., Brilke, S., Murillo, L. C., Chiu, R., Chu, B., De Menezes, L.-P., Duplissy, J., Finkenzeller, H., Carracedo, L. G., Granzin, M., Guida, R., Hansel, A., Hofbauer, V., Krechmer, J., Lehtipalo, K., Lamkaddam, H., Lampimäki, M., Lee, C. P., Makhmutov, V., Marie, G., Mathot, S., Mauldin, R. L., Mentler, B., Müller, T., Onnela, A., Partoll, E., Petäjä, T., Philippov, M., Pospisilova, V., Ranjithkumar, A., Rissanen, M., Rörup, B., Scholz, W., Shen, J., Simon, M., Sipilä, M., Steiner, G., Stolzenburg, D., Tham, Y. J., Tomé, A., Wagner, A. C., Wang, D. S., Wang, Y., Weber, S. K., Winkler, P. M., Wlasits, P. J., Wu, Y., Xiao, M., Ye, Q., Zauner-Wieczorek, M., Zhou, X., Volkamer, R., Riipinen, I., Dommen, J., Curtius, J., Baltensperger, U., Kulmala, M., Worsnop, D. R., Kirkby, J., Seinfeld, J. H., El-Haddad, I., Flagan, R. C. and Donahue, N. M.: Rapid growth of new atmospheric particles by nitric acid and ammonia condensation, *Nature*, 581(7807), 184–189, doi:10.1038/s41586-020-2270-4, 2020d.

Wang, X., Wang, T., Yan, C., Tham, Y. J., Xue, L., Xu, Z. and Zha, Q.: Large daytime signals of N₂O₅ and NO₃ inferred at 62 amu in a TD-CIMS: Chemical interference or a real atmospheric phenomenon, *Atmospheric Measurement Techniques*, 7(1), 1–12, doi:10.5194/amt-7-1-2014, 2014b.

Wang, Y., Riva, M., Xie, H. and Heikkinen, L.: Formation of highly oxygenated organic molecules from chlorine atom initiated oxidation of alpha-pinene, *Atmospheric Chemistry and Physics*, 2020, 1–31, doi:10.5194/acp-2019-807, 2020.

Wang, Y., Wang, Y., Wang, L., Petäjä, T., Zha, Q., Gong, C., Li, S., Pan, Y., Hu, B., Xin, J. and Kulmala, M.: Increased inorganic aerosol fraction contributes to air pollution and haze in China, *Atmos. Chem. Phys.*, 19, 5881–5888, doi:10.5194/acp-19-5881-2019, 2019b.

Wang, Y., Gao, W., Wang, S., Song, T., Gong, Z., Ji, D., Wang, L., Liu, Z., Tang, G., Huo, Y., Tian, S., Li, J., Li, M., Yang, Y., Chu, B., Petäjä, T., Kerminen, V.-M., He, H., Hao, J., Kulmala,

- M., Wang, Y. and Zhang, Y.: Contrasting trends of PM_{2.5} and surface ozone concentrations in China from 2013 to 2017, *National Science Review*, doi:10.1093/nsr/nwaa032, 2020b.
- Wang, Y., Chen, Y., Wu, Z., Shang, D., Bian, Y., Du, Z. and Schmitt, S. H.: Mutual promotion between aerosol particle liquid water and particulate nitrate enhancement leads to severe nitrate-dominated particulate matter pollution and low visibility, *Atmos. Chem. Phys.*, (September 2020), 2161–2175, 2020c.
- Wang, Y., Yu, M., Wang, Y., Tang, G., Song, T., Zhou, P., Liu, Z., Hu, B., Ji, D., Wang, L., Zhu, X., Yan, C., Ehn, M., Gao, W., Pan, Y., Xin, J., Sun, Y., Kerminen, V.-M., Kulmala, M. and Petäjä, T.: Rapid formation of intense haze episodes via aerosol–boundary layer feedback in Beijing, *Atmos. Chem. Phys.*, 20(1), 45–53, doi:10.5194/acp-20-45-2020, 2020d.
- Wang, Y. H., Hu, B., Ji, D. S., Liu, Z. R., Tang, G. Q., Xin, J. Y., Zhang, H. X., Song, T., Wang, L. L., Gao, W. K., Wang, X. K. and Wang, Y. S.: Ozone weekend effects in the Beijing-Tianjin-Hebei metropolitan area, China, *Atmos. Chem. Phys.*, 14, 2419–2429, doi:10.5194/acp-14-2419-2014, 2014c.
- Wang, Y. H., Liu, Z. R., Zhang, J. K., Hu, B., Ji, D. S., Yu, Y. C. and Wang, Y. S.: Aerosol physicochemical properties and implications for visibility during an intense haze episode during winter in Beijing, *Atmospheric Chemistry and Physics*, 15(6), 3205–3215, doi:10.5194/acp-15-3205-2015, 2015.
- Wu, Z., Wang, Y., Tan, T., Zhu, Y., Li, M., Shang, D., Wang, H., Lu, K., Guo, S., Zeng, L. and Zhang, Y.: Aerosol Liquid Water Driven by Anthropogenic Inorganic Salts: Implying Its Key Role in Haze Formation over the North China Plain, *Environmental Science and Technology Letters*, 5(3), 160–166, doi:10.1021/acs.estlett.8b00021, 2018.
- Xie, Y., Ding, A., Nie, W., Mao, H., Qi, X., Huang, X., Xu, Z., Kerminen, V. M., Petäjä, T., Chi, X., Virkkula, A., Boy, M., Xue, L., Guo, J., Sun, J., Yang, X., Kulmala, M. and Fu, C.: Enhanced sulfate formation by nitrogen dioxide: Implications from in-situ observations at the SORPES station, *Journal of Geophysical Research*, 120(24), 12,679–12,694, doi:10.1002/2015JD023607, 2015.
- Xue, J., Yuan, Z., Griffith, S. M., Yu, X., Lau, A. K. H. and Yu, J. Z.: Sulfate Formation Enhanced

by a Cocktail of High NO_x, SO₂, Particulate Matter, and Droplet pH during Haze-Fog Events in Megacities in China: An Observation-Based Modeling Investigation, *Environmental Science and Technology*, 50(14), 7325–7334, doi:10.1021/acs.est.6b00768, 2016.

Xue, J., Yu, X., Yuan, Z., Griffith, S. M., Lau, A. K. H., Seinfeld, J. H. and Yu, J. Z.: Efficient control of atmospheric sulfate production based on three formation regimes, *Nature Geoscience*, 12(12), 1–6, doi:10.1038/s41561-019-0485-5, 2019.

Zheng, B., Tong, D., Li, M., Liu, F., Hong, C., Geng, G., Li, H., Li, X., Peng, L., Qi, J., Yan, L., Zhang, Y., Zhao, H., Zheng, Y., He, K. and Zhang, Q.: Trends in China's anthropogenic emissions since 2010 as the consequence of clean air actions, *Atmospheric Chemistry and Physics Discussions*, 1–27, doi:10.5194/acp-2018-374, 2018.

Zhong, J., Zhang, X., Dong, Y., Wang, Y., Liu, C., Wang, J., Zhang, Y. and Che, H.: Feedback effects of boundary-layer meteorological factors on cumulative explosive growth of PM_{2.5} during winter heavy pollution episodes in Beijing from 2013 to 2016, *Atmospheric Chemistry and Physics*, 18(1), 247–258, doi:10.5194/acp-18-247-2018, 2018.

Zhou, Y., Dada, L., Liu, Y., Fu, Y., Kangasluoma, J., Chan, T., Yan, C., Chu, B., Daellenbach, K. R., Bianchi, F., Kokkonen, T. V., Liu, Y., Kujansuu, J., Kerminen, V.-M., Petäjä, T., Wang, L., Jiang, J. and Kulmala, M.: Variation of size-segregated particle number concentrations in wintertime Beijing, *Atmospheric Chemistry and Physics*, 20(2), 1201–1216, doi:10.5194/acp-20-1201-2020, 2020.

421

422

423

424

425

426

427

428

429

Figure caption

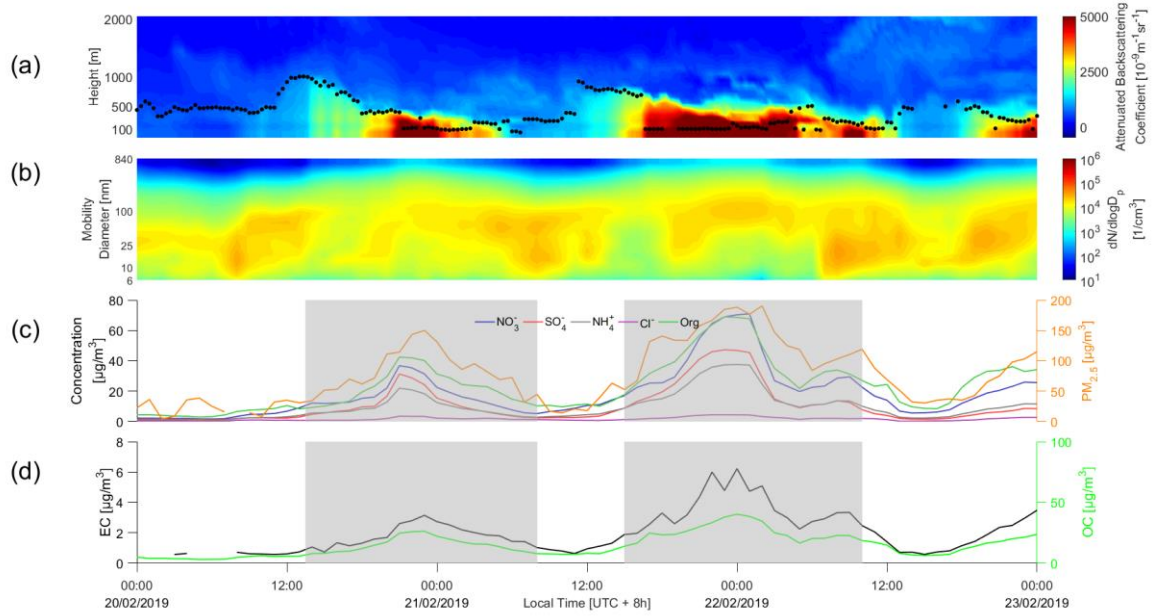


Figure 1. Time series of (a) attenuated backscattering coefficient and mixing layer height (b) particle number concentration distribution (PNSD), (c) chemical composition and $\text{PM}_{2.5}$ mass concentrations and (d) elemental carbon (EC) and organic carbon (OC). The haze periods are marked by the shaded areas.

449
450

451
452
453
454
455
456
457
458
459
460
461
462
463
464
465

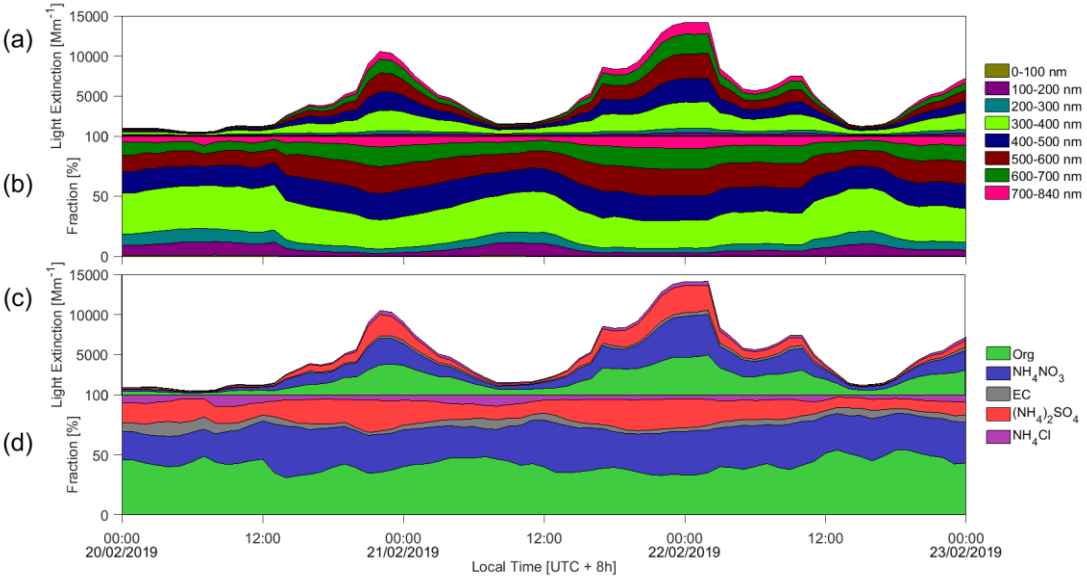


Figure 2. Time series of (a, b) variation of light extinction from different size aerosol and fractions, and (c, d) variation of light extinction from different aerosol species and fractions. The legends in the left side of figures are particle diameter and the right side are chemical compositions, respectively.

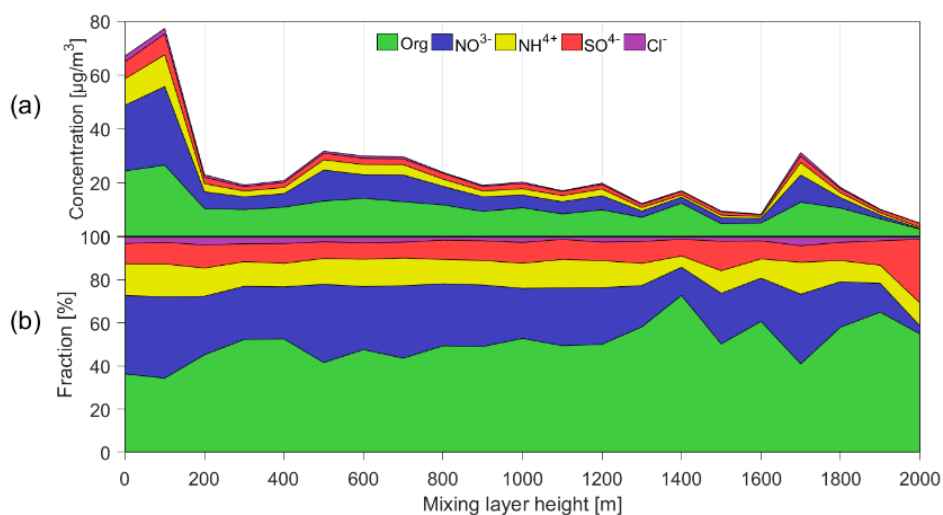


Figure 3. Statistical relationship between MLH and concentration (a) and fraction (b) of chemical composition species. Only daytime conditions determined by ceilometer from non-rainy periods (RH<95%) during the observation (~ 6 months) are considered.

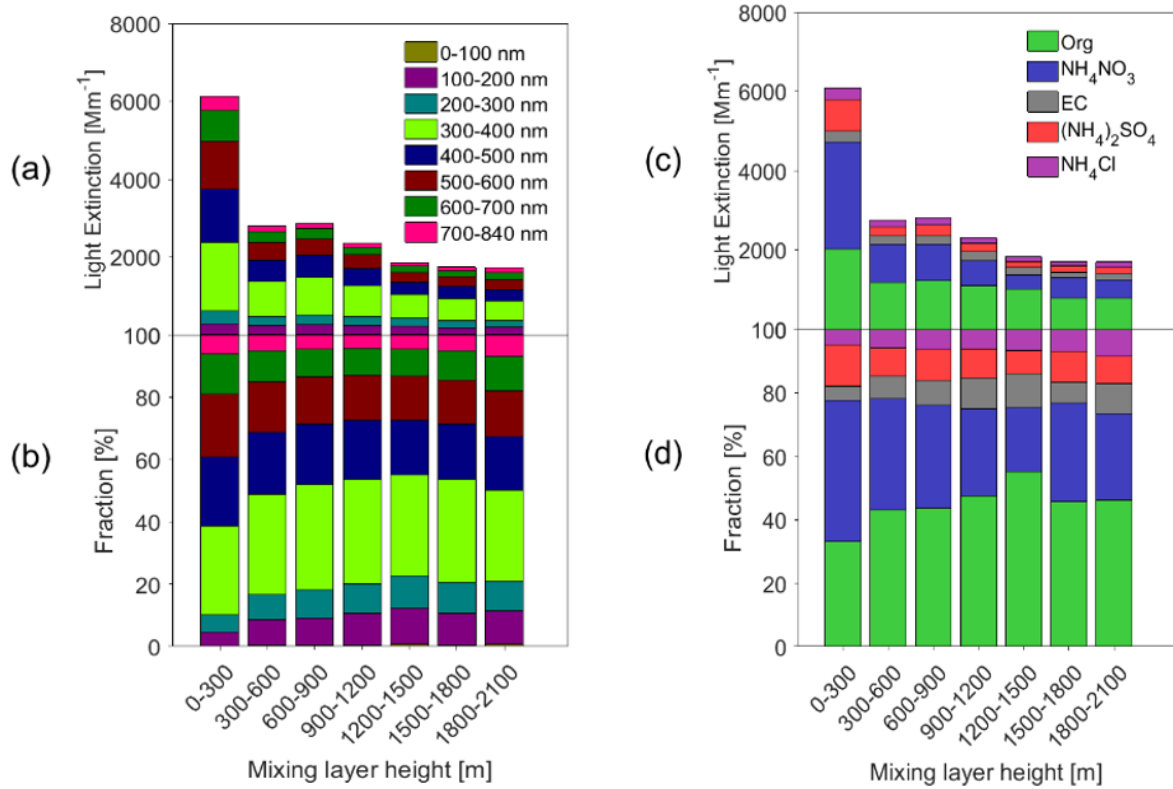
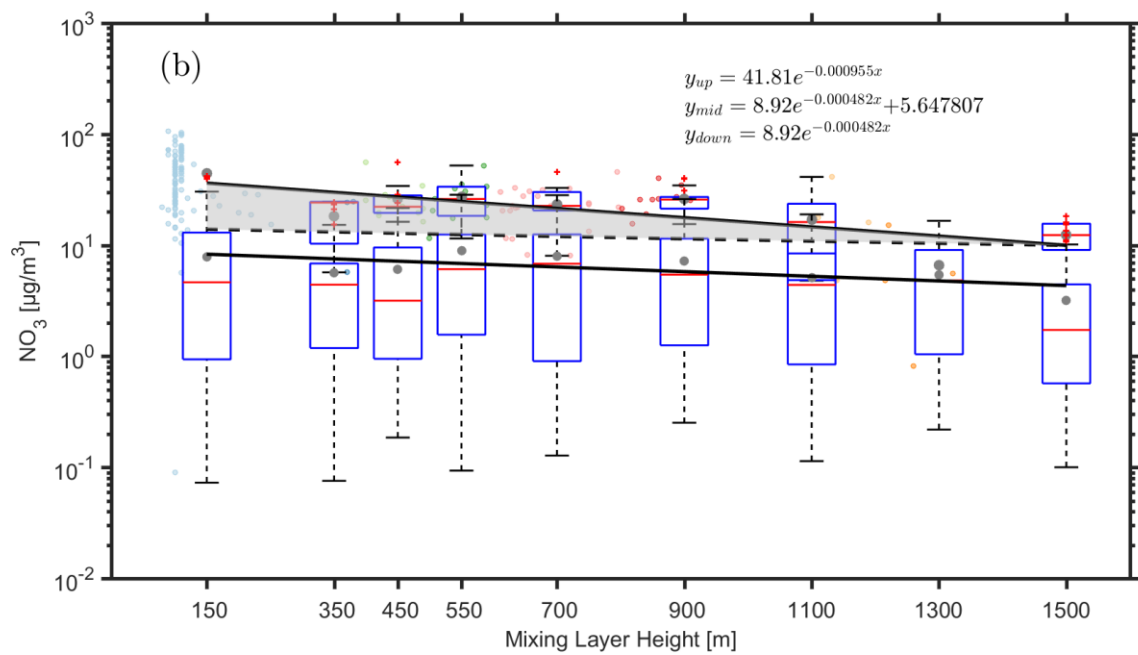
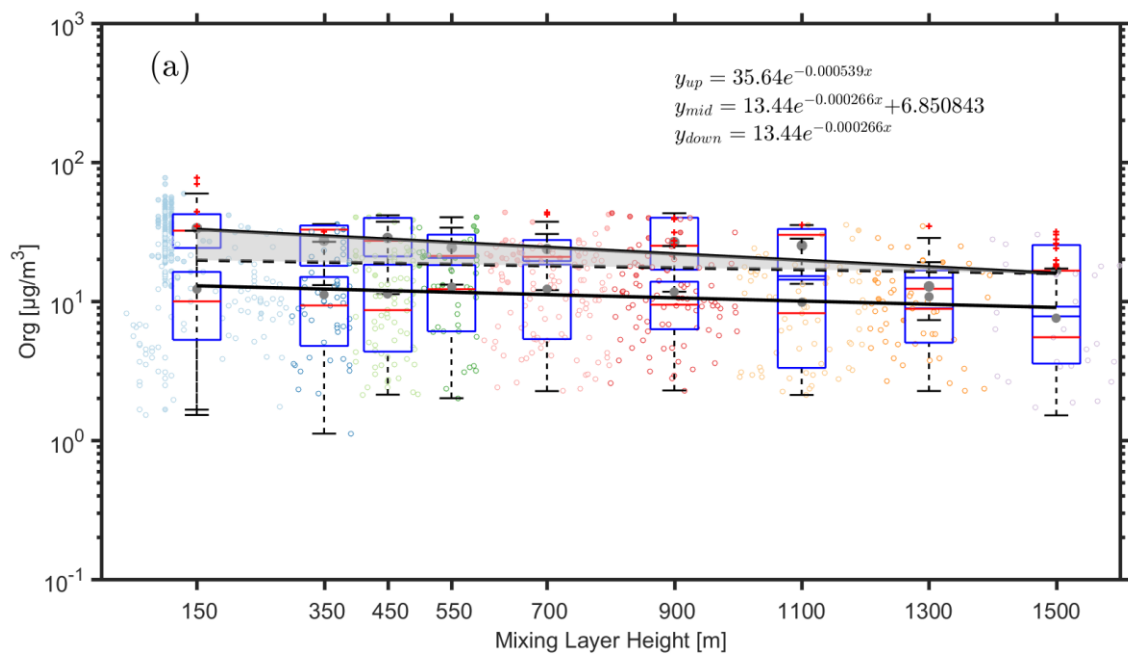
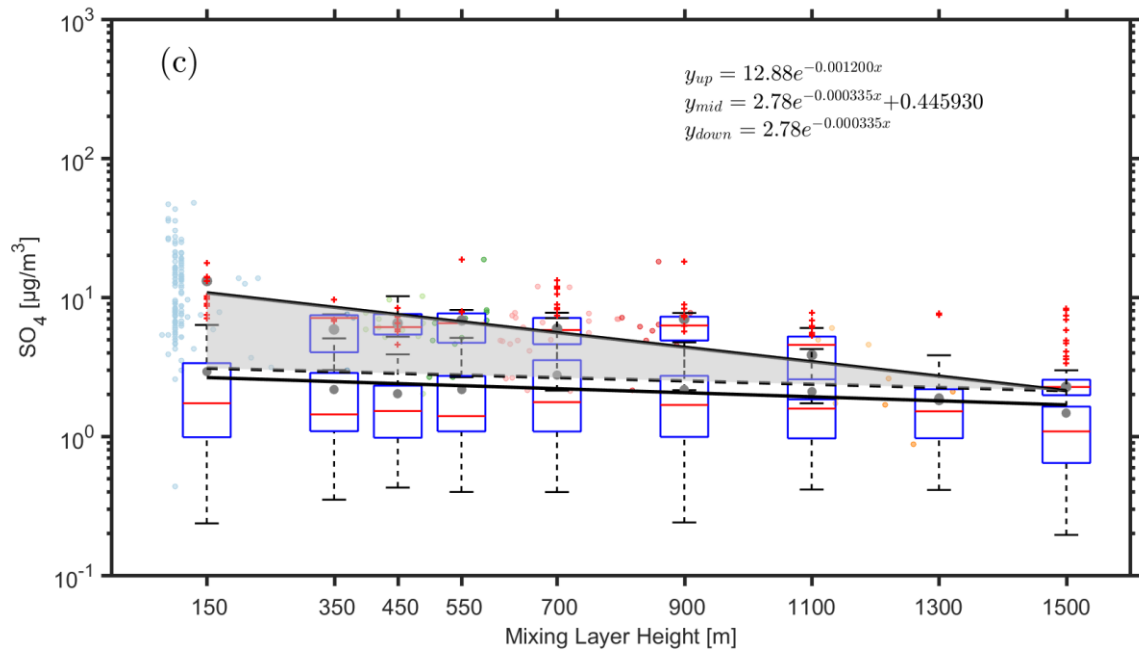


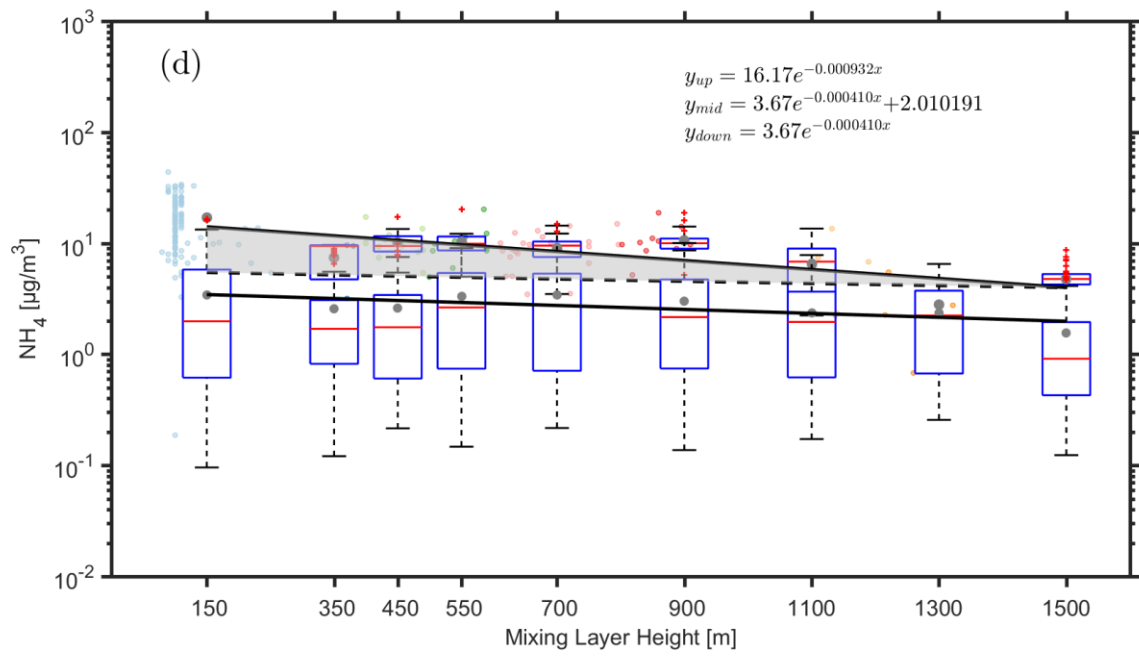
Figure 4. Statistical relationship between MLH and light extinction of different aerosol species. Only daytime conditions determined by the ceilometer from non-rainy periods ($\text{RH} < 95\%$) are considered.

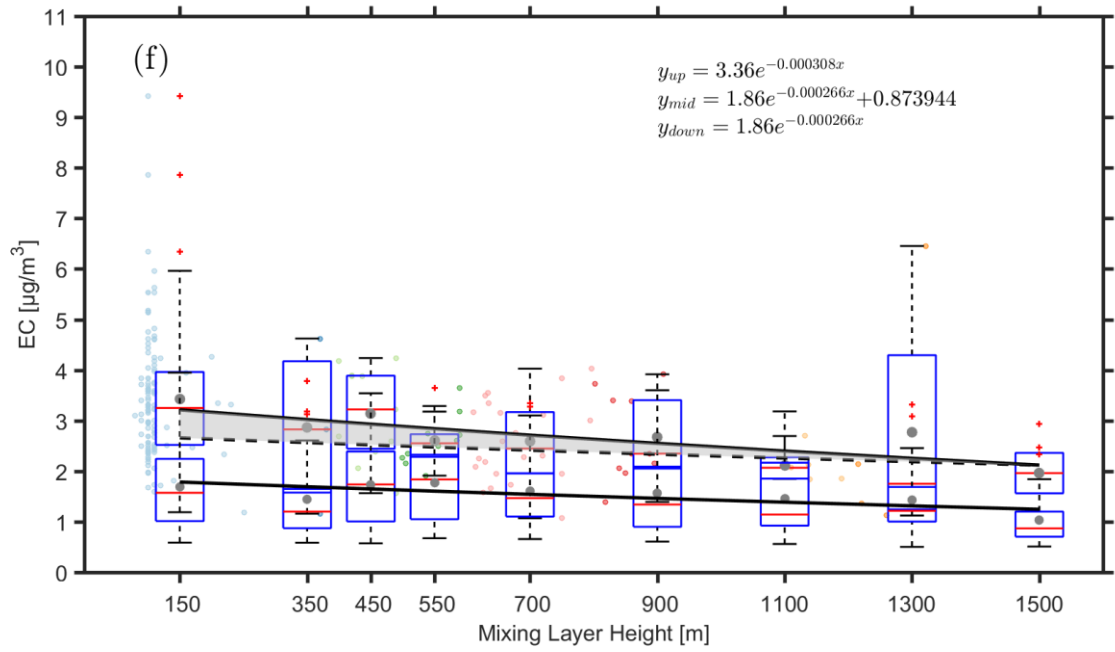
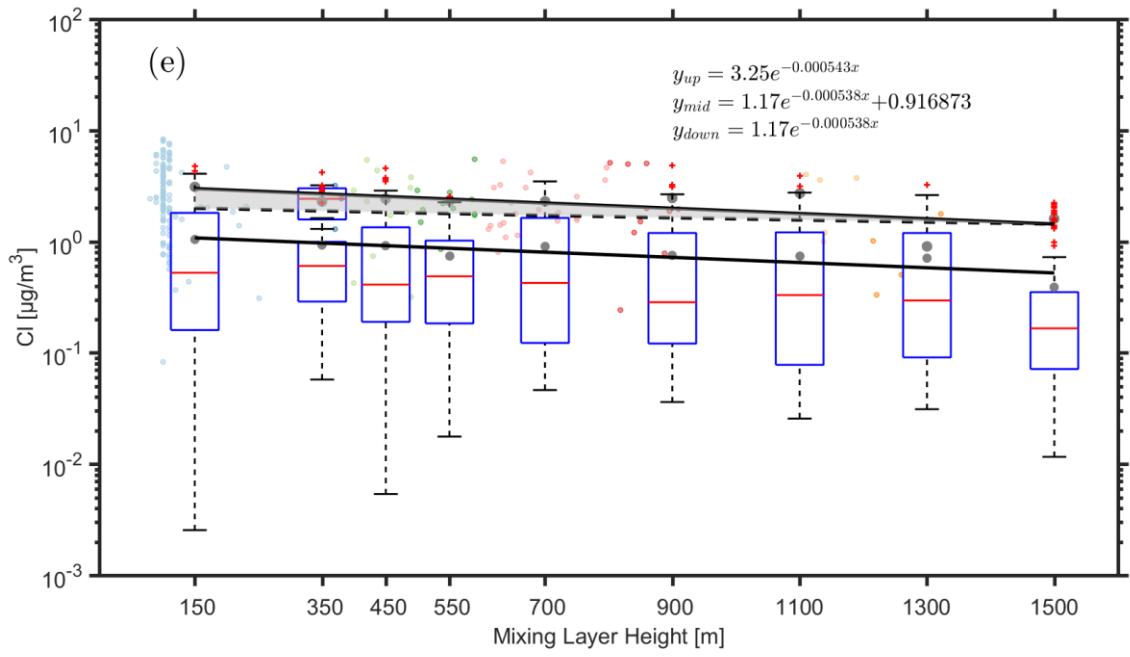


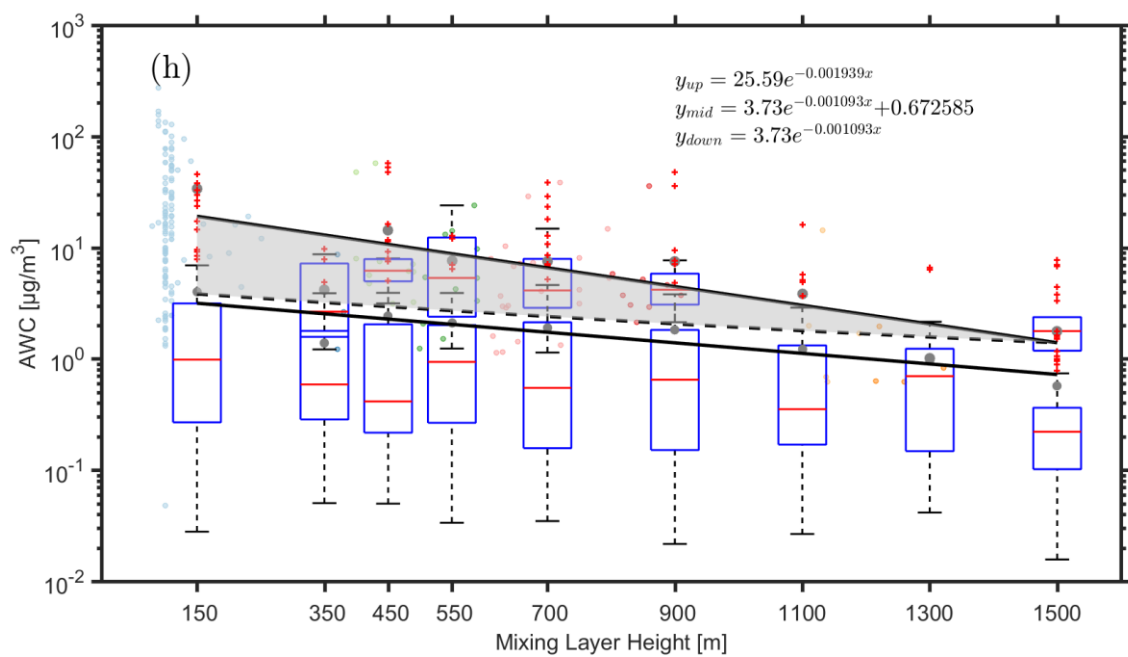
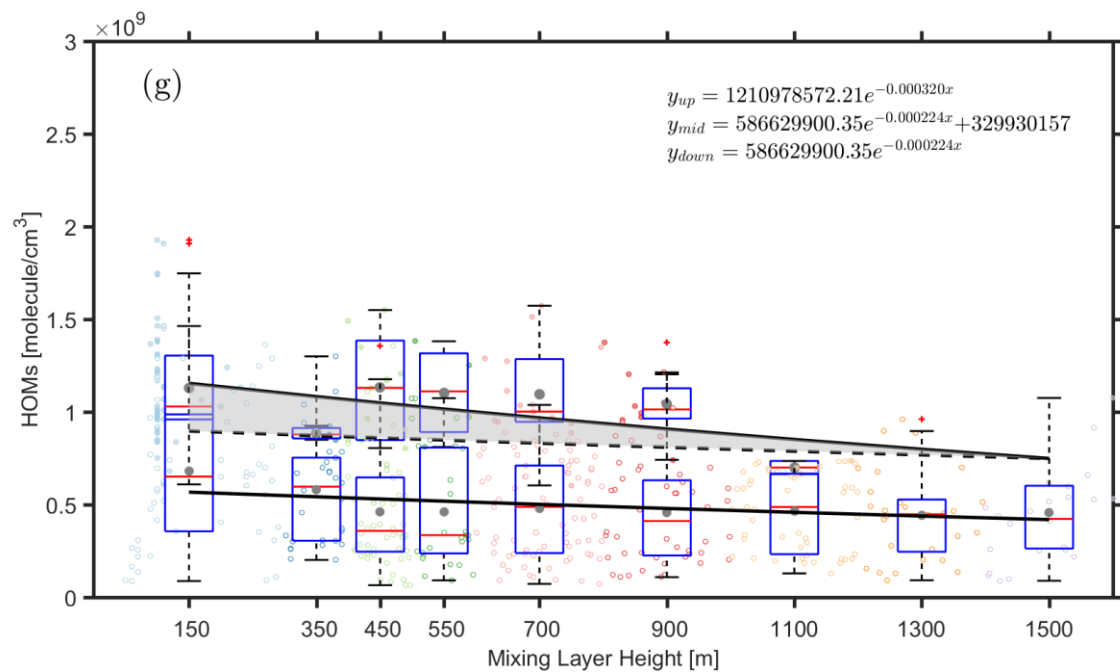
500



501







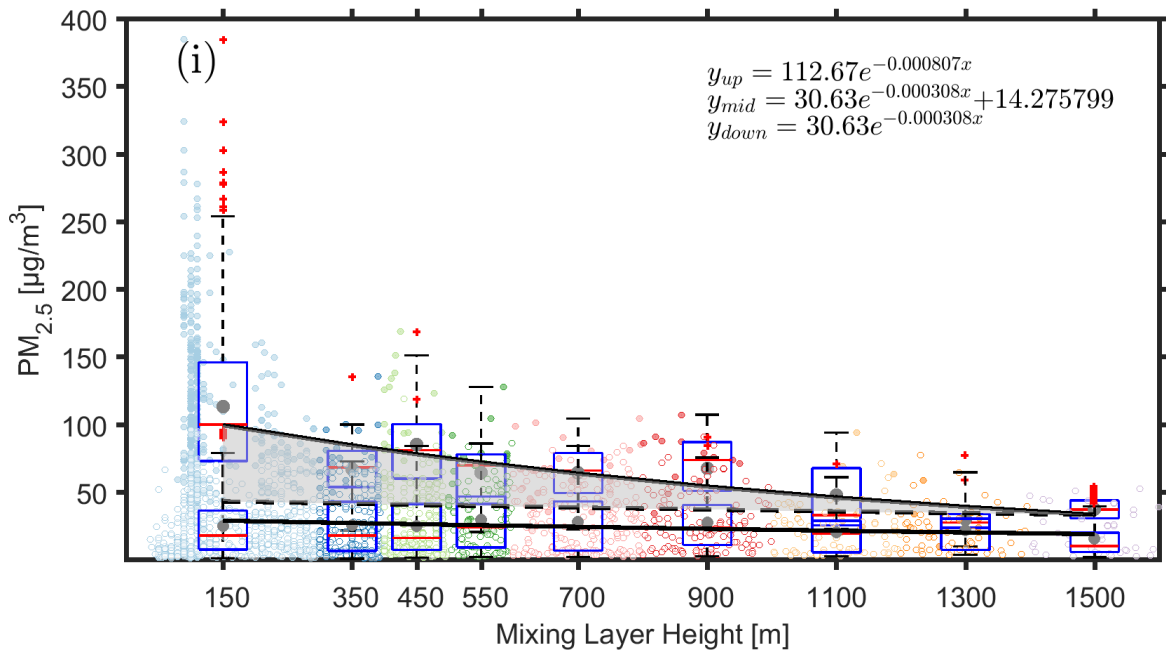
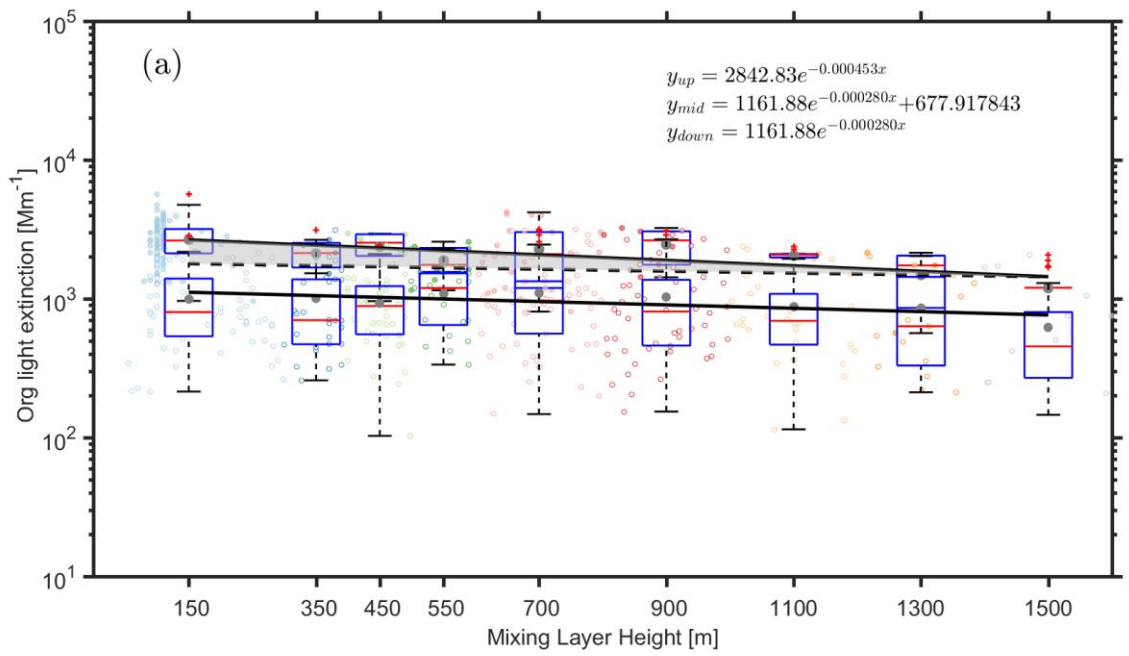
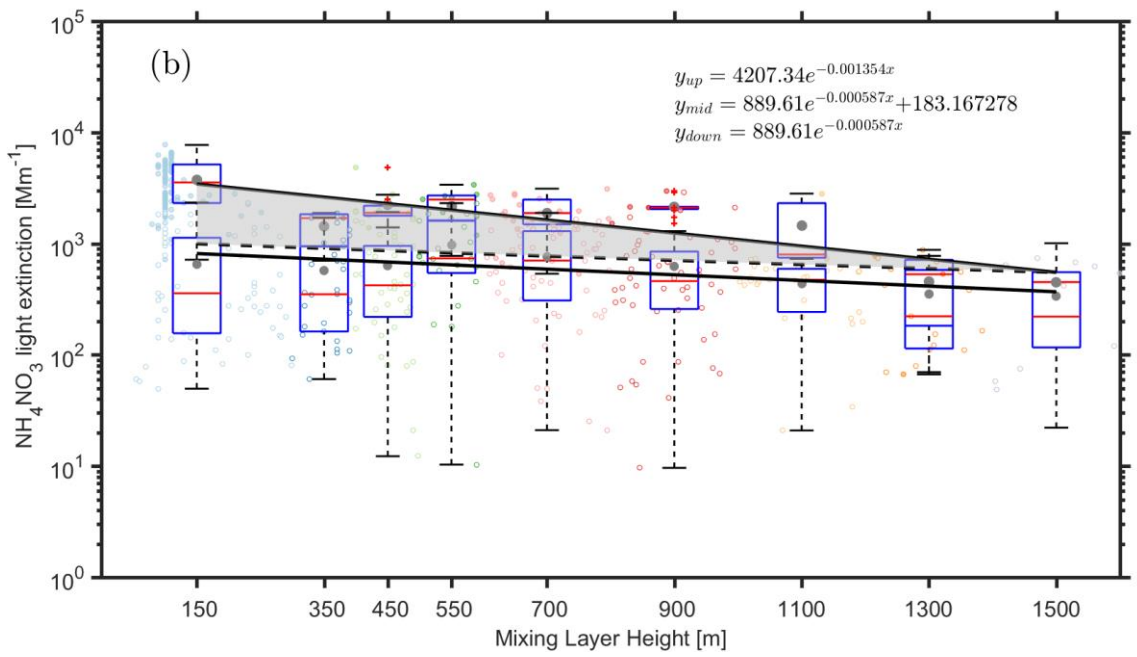


Figure 5. Observed dependency of (organics (a), nitrate (b), ammonium (c), sulfate (d), chlorine (e), element carbon (f), HOMs (g), AWC (h) and PM_{2.5}(i) on the MLH during polluted and less-polluted conditions. The data related to the upper fitting line represents PM_{2.5} concentrations larger than 75 µg m⁻³, while the data related to the lower fitting line represents PM_{2.5} concentrations lower than 75 µg m⁻³. Only daytime conditions determined by the ceilometer from non-rainy periods (RH<95%) were considered. The solid cycles and hollow cycles denotes concentrations that are more than 75 µg m⁻³ and less than 75 µg m⁻³, respectively. The dark grey points and red lines in the boxes represent mean and median values, respectively. The shaded area between the upper solid and dotted lines corresponds to an increased amount of the specific compounds with decreased MLH, assuming that the compound has the same variation pattern under highly- polluted conditions as in less polluted time.

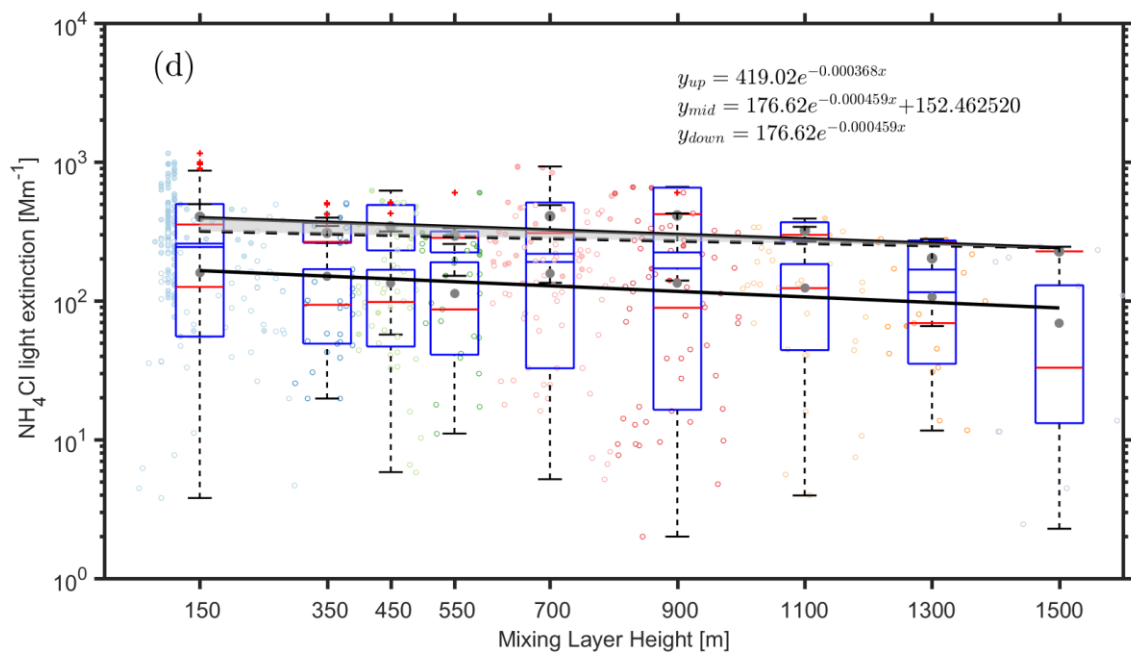
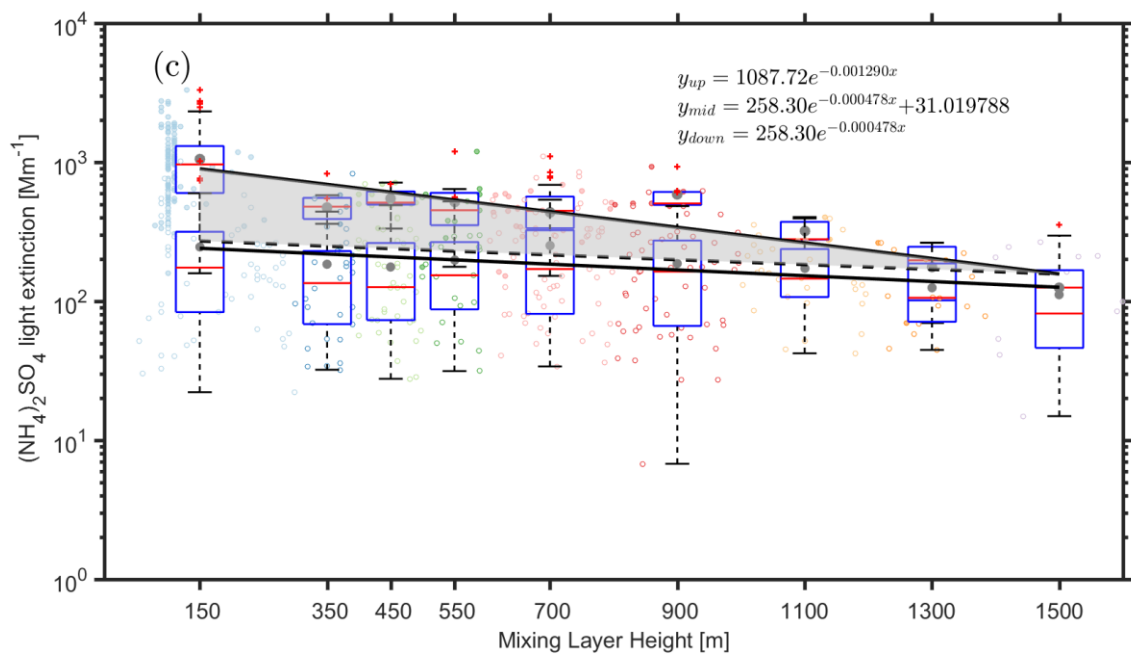
528
529
530



531



532



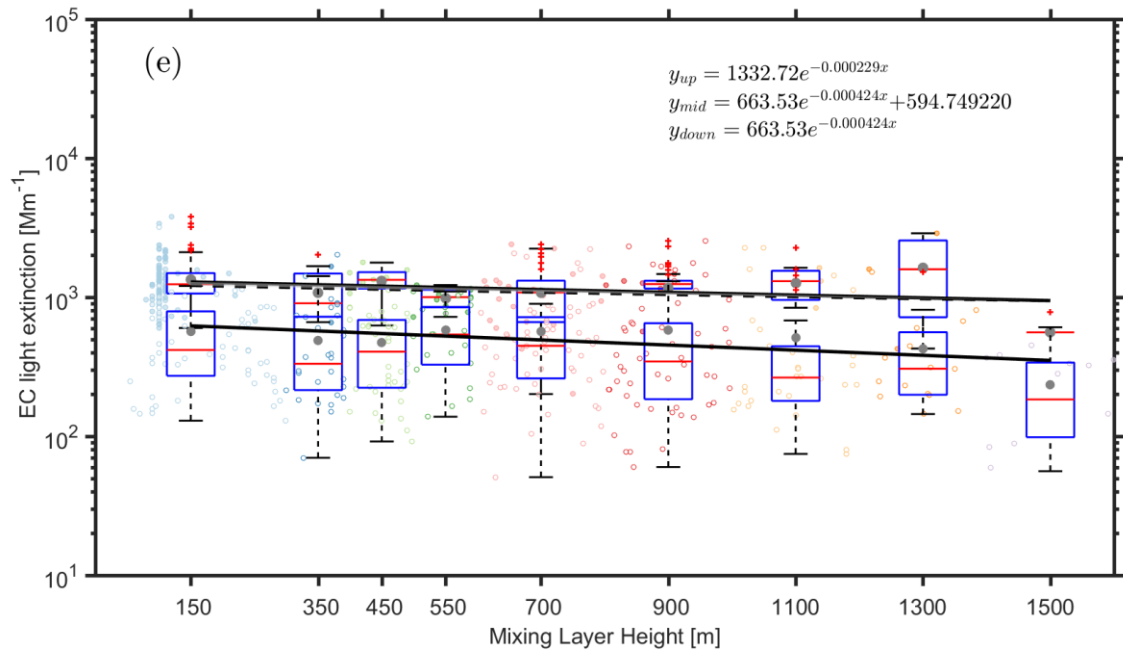


Figure 6. Observed dependency of the aerosol light extinction due to NH_4NO_3 (a) $(\text{NH}_4)_2\text{SO}_4$ (b), NH_4Cl (c) Org (d) and EC (e) on the MLH during polluted and non-polluted conditions. The data related to the upper fitting line represents $\text{PM}_{2.5}$ concentrations larger than $75 \mu\text{g m}^{-3}$, while the data related to the lower fitting line represents $\text{PM}_{2.5}$ concentrations less than $75 \mu\text{g m}^{-3}$. Only daytime conditions determined by ceilometer from non-rainy periods ($\text{RH} < 95\%$) are considered. The dark grey points and red lines in the boxes represent mean and median values, respectively. The shaded area between the upper solid and dashed line corresponds to an increased amount of $\text{PM}_{2.5}$ with a decreased MLH, assuming that $\text{PM}_{2.5}$ has the same variation pattern under highly- polluted conditions as in less polluted time

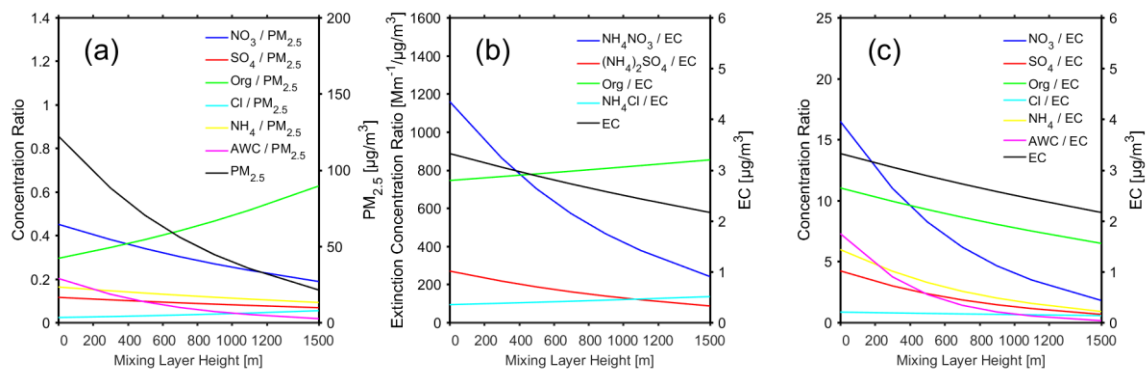


Figure 7. (a) the ratio of the mass concentration of different chemical components (nitrate, sulfate, organics, chlorine, ammonium) and AWC to the mass concentration of NR_PM_{2.5} as a function of MLH. (b) the ratio of dry aerosol light extinction by different chemical components (NH₄NO₃, (NH₄)₂SO₄, Org, NH₄Cl) to the mass concentration EC as a function of MLH (c) the ratio of the mass concentration of different chemical components (nitrate, sulfate, organics, chlorine, ammonium) and AWC to the mass concentration of EC as a function of MLH. All the data corresponds to polluted conditions (fine PM > 75 $\mu\text{g}/\text{m}^3$), and only daytime conditions determined by the ceilometer from non-rainy periods (RH < 95%) were considered.

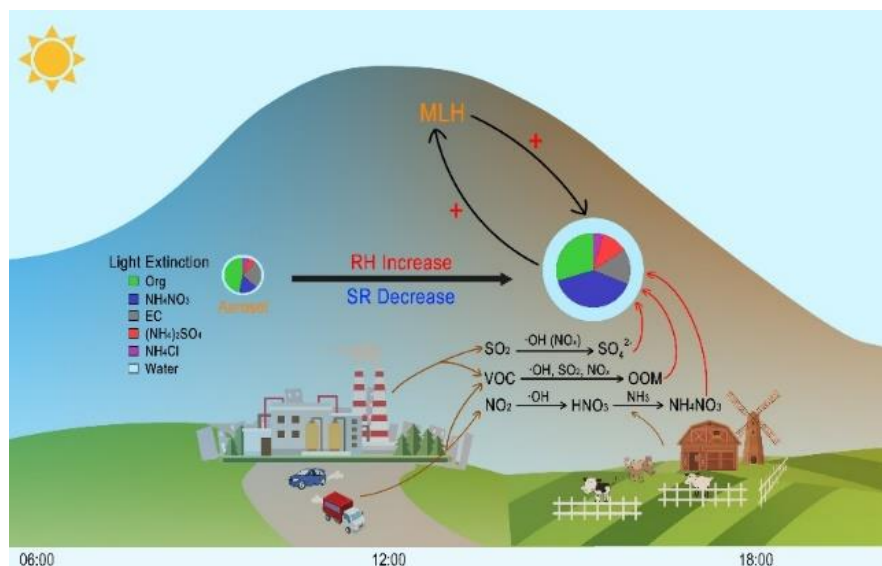


Figure 8. A schematic picture illustrating the process of rapid aerosol mass growth and enhanced light extinction in Beijing. The plus symbols represent the strengthening of a specific process. At the presence of aerosols during afternoon time in Beijing, the intensity of solar radiation reaching the surface will be decreased and relative humidity will be increased. As a result, the development of boundary layer will be suppressed, and the concentrations of aerosol precursors (e.g., SO_2 , NO_2 , VOC) will be increased. In turn, the secondary production of these sulfate, nitrate and oxygenated organic compounds will be enhanced due to increased concentrations and partitioning of these compounds into the aerosol phase. The increased formation of secondary aerosol mass will reduce solar radiation further and the haze formation increased, as shown in pie charts that the light extinction fraction of aerosol changed from organic to nitrate. Noting that during intensive haze periods, nitrate and its contribution to light extinction contribution increased dramatically.